



**HAL**  
open science

# Optimization of a radiative membrane for gas sensing applications

Anthony Lefebvre, Salim Boutami, Jean-Jacques Greffet, H. Benisty

► **To cite this version:**

Anthony Lefebvre, Salim Boutami, Jean-Jacques Greffet, H. Benisty. Optimization of a radiative membrane for gas sensing applications. Photonics Europe, Optical Sensing and Detection, Society of Photo-Optical Instrumentation Engineers (SPIE), Apr 2014, Brussels, Belgium. 10.1117/12.2052273 . hal-01659635

**HAL Id: hal-01659635**

**<https://hal.science/hal-01659635>**

Submitted on 30 Aug 2022

**HAL** is a multi-disciplinary open access archive for the deposit and dissemination of scientific research documents, whether they are published or not. The documents may come from teaching and research institutions in France or abroad, or from public or private research centers.

L'archive ouverte pluridisciplinaire **HAL**, est destinée au dépôt et à la diffusion de documents scientifiques de niveau recherche, publiés ou non, émanant des établissements d'enseignement et de recherche français ou étrangers, des laboratoires publics ou privés.

# Optimization of a radiative membrane for gas sensing applications

Anthony Lefebvre<sup>\*a,b</sup>, Salim Boutami<sup>a</sup>, Jean-Jacques Greffet<sup>b</sup>, Henri Benisty<sup>b</sup>

<sup>a</sup>CEA, LETI, MINATEC Campus, 17 rue des Martyrs, F-38054 Grenoble Cedex 9, France

<sup>b</sup>Laboratoire Charles Fabry, Institut d'Optique, CNRS, Univ Paris Sud, 2, Avenue Augustin Fresnel, 91127 Palaiseau cedex, France

## ABSTRACT

To engineer a cheap, portable and low-power optical gas sensor, incandescent sources are more suitable than expensive quantum cascade lasers and low-efficiency light-emitting diodes. Such sources of radiation have already been realized, using standard MEMS technology, consisting in free standing circular micro-hotplates. This paper deals with the design of such membranes in order to maximize their wall-plug efficiency. Specification constraints are taken into account, including available energy per measurement and maximum power delivered by the electrical supply source. The main drawback of these membranes is known to be the power lost through conduction to the substrate, thus not converted in (useful) radiated power. If the membrane temperature is capped by technological requirements, radiative flux can be favored by increasing the membrane radius. However, given a finite amount of energy, the larger the membrane and its heat capacity, the shorter the time it can be turned on. This clearly suggests that an efficiency optimum has to be found. Using simulations based on a spatio-temporal radial profile, we demonstrate how to optimally design such membrane systems, and provide an insight into the thermo-optical mechanisms governing this kind of devices, resulting in a non-trivial design with a substantial benefit over existing systems. To further improve the source, we also consider tailoring the membrane stack spectral emissivity to promote the infrared signal to be sensed as well as to maximize energy efficiency.

**Keywords:** gas sensing, MEMS, membrane, spectral efficiency

\*[anthony.lefebvre@cea.fr](mailto:anthony.lefebvre@cea.fr)

## 1. INTRODUCTION

Optical gas sensing is a key technology enabling the detection and concentration measurement of gaseous chemical species. It is used in a wide variety of applications, including, but not limited to: industrial process control, air quality monitoring, gas leak detection, hazardous/pollutant gas sensing... Different technologies have been developed, among which NDIR (Non-Dispersive InfraRed) sensors, which have been particularly investigated recently. This kind of optical detectors rely on the unique fingerprint most gases exhibit in the infrared (IR) range, related to their rotational-vibrational molecular energy ladder. The gas of interest is located in a cavity and is probed by an IR source, either a blackbody or a quantum cascade laser, depending on the applications. The power attenuation measured by a detector provides the gas concentration according to the Beer-Lambert law:

$$P = P_0 \int_{\Delta\lambda} 10^{-\epsilon(\lambda)lc} d\lambda \quad (1)$$

where  $P$  is the measured power,  $P_0$  is the reference power in the absence of gas,  $l$  is the path length through the gas, and  $\epsilon$  and  $c$  are respectively the molar absorptivity and the molar concentration of the gas. The integration over  $\Delta\lambda$  is related to the spectral bandwidth of the measured signal, usually truncated by a filter.

The radiation source plays an important role both in the overall sensor wall-plug efficiency and in its cost since detectors, e.g. pyroelectric ones, usually are high impedance devices. In order to design a cheap, low-consumption gas sensor, the source has to be carefully optimized. The price issue has been successfully dealt with by using MEMs technology, which strongly reduces manufacturing costs. The standard realization for these wafer-level sources is the suspended micromembrane, or microbridge. The idea behind these designs is to insulate the heat source from the substrate, to reduce losses. These structures have been widely studied since the late 1980s<sup>1,2</sup>. Ali *et al.* provided an extensive review of latest achievements in this domain<sup>3</sup>. Principal concerns are power reduction, mechanical stability, durability and

CMOS compatibility. Recently, analytical models have also been introduced to enhance the temperature homogeneity, which is an important feature for efficient sources<sup>4,6</sup>. In this paper, we propose an in-depth comprehensive study of the thermo-optical phenomena occurring in these membranes, when application-oriented energetic constraints are taken into account. For generality, we use a simplified model and a rather generic source.

## 2. MEMBRANE MODELING

### 2.1 Geometrical model

We consider a standard suspended micromembrane, made of a wire-like metallic resistive heater surrounded by a robust shell of dielectric material. Temperature uniformity is guaranteed by homogenizing spacers between wires, made from the same material as the heaters, but electrically isolated by very narrow trenches. In order to simplify the geometry, a certain number of hypotheses are made, illustrated on Figure 1. We consider the membrane thickness  $e$  to be much smaller than its radius  $R$ , allowing the temperature to be independent of the height (Fig. 1.a and Fig. 1.b). Given obvious symmetry considerations, we only consider a fourth of the membrane. The geometry is also further reduced to a one-dimensional radial problem, assuming a rotational invariance (hence looking like Fig. 1.c and Fig. 1.d). We justify this assumption by homogenizing the arms versus the azimuthal variable  $\theta$ , some more details being given later. In particular the same thermal conductance is retained if the “extended arms” thermal characteristics of the model are those of the real arms multiplied by the relative weight of their intersection with the perimeter of the membrane. No corrections are made for metallic tracks that cover almost  $2\pi$  azimuth. Finally, we consider that the whole central disk is made of a single material, justified by the small size of its heating tracks (see Fig. 1.d and Fig. 1.e). The complex problem of a three-dimensional suspended membrane is thus reduced to a simple bi-material one-dimensional problem, without much loss of generality.

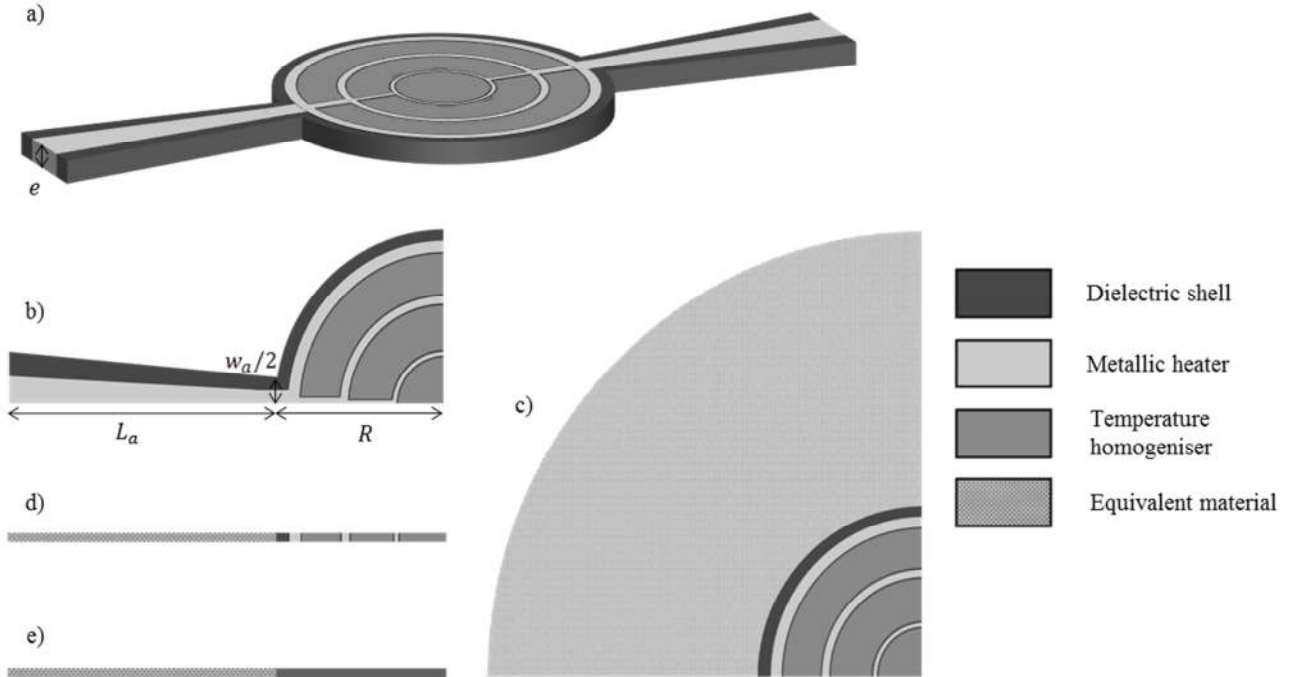


Figure 1: a) Complete 3D suspended membrane, including metallic heaters, temperature homogenizers, and dielectric shell. Here we consider two suspension arms. b) 2D reduced model, neglecting the vertical expansion of the structure. c) Azimuthally invariant model. The metallic tracks variations are neglected and the arms are homogenized to be redistributed around the membrane, using an equivalent material which retains the correct overall conductance. d) 1D radial model, derived from the rotational invariance of figure c). e) 1D model considering a homogeneous central disk.

## 2.2 Thermal model

The micro-hotplate is composed of two different parts: a central heating core of radius  $R$  and a set of  $N_a$  arms of length  $L_a$  and width  $w_a$  (measured on disk perimeter) allowing the suspension (Figure 1). According to Stefan-Boltzmann's law, the radiative power of a blackbody is expressed as  $P = S\sigma T^4$ , with  $\sigma$  the Stefan-Boltzmann constant and  $S$  the surface of the blackbody. Given the small surface of the arms and their low temperature compared to the core, they play very little role in the total radiation. As a consequence, they can be considered as a simple thermal leakage resistance  $Z_a$ , defined by:

$$Z_a = \frac{L_a}{\kappa'_a} = \frac{L_a}{\kappa_a \frac{N_a w_a}{2\pi R}} \quad [\text{K} \cdot \text{W}^{-1} \cdot \text{m}^2] \quad (2)$$

where  $L_a$  is the length of the arms and  $\kappa'_a$  is the equivalent thermal conductivity, obtained from the arms thermal conductivity  $\kappa_a$  weighted by their relative intersection with the perimeter of the membrane  $N_a w_a / 2\pi R$ . In the following calculations, we consider a constant value of  $Z_a$ , to focus on the phenomena taking place in the central disk. It means that when this disk radius increases, the width of the arms  $w_a$  increases accordingly, to guarantee the constancy of  $\kappa'_a$ . The length of the arms thus remains the same.

Using this simple model, cylindrical thermal equations with source terms can be implemented as:

$$\rho C_p \frac{\partial T(r, t)}{\partial t} = \kappa \left( \frac{\partial^2 T(r, t)}{\partial r^2} + \frac{1}{r} \frac{\partial T(r, t)}{\partial r} \right) - \frac{1}{e} 2\varphi_{rad}(T(r, t)) + P(t) \quad (3)$$

with

$$\varphi_{rad}(T(r, t)) = \pi \int_0^\infty \varepsilon(\lambda) \left[ I(\lambda, T(r, t)) - I(\lambda, T_{sub}(r, t)) \right] d\lambda \quad (4)$$

where  $\rho$  is the mass density,  $C_p$  is the specific heat capacity,  $\kappa$  is the thermal conductivity,  $\varepsilon$  is the emissivity of the material and  $I$  stands for the spectral radiance of the blackbody, given by Planck's law. We neglect a possible angular dependence of radiation that is possible in thin stratified media. The factor 2 applied to  $\varphi_{rad}$  in expression (5) stands for the emission on both faces of the membrane. We are interested in solving equation (3) to find the spatio-temporal distribution of temperature  $T(r, t)$ . Convection is neglected, as we assume the microsource to be vacuum-encapsulated. The heat source  $P(t)$  is approximated by an even distribution on the central disk of the membrane, which is valid when using temperature homogenisers. Initially, the whole membrane is at the cold MEMS substrate temperature  $T_{sub}$ :  $T(r, 0) = T_{sub}$ . The boundary conditions are given by:

$$-\kappa \frac{\partial T(0, t)}{\partial r} = 0 \quad (6)$$

$$-\kappa \frac{\partial T(R, t)}{\partial r} = \frac{1}{Z_a e} (T(R, t) - T_{sub}) \quad (7)$$

Equation (6) is a Neumann condition at  $r = 0$  imposed by the axisymmetry. Equation (7) is a Robin condition at  $r = R$  imposed through the arms thermal resistance. The substrate is considered to be a thermostat at  $T_{sub}$ .

## 3. MEMBRANE OPTIMISATION

### 3.1 General context

Our goal is to maximize the wall-plug efficiency of the membrane, that is the conversion from electrical to optical radiative energy. Moreover, as we target gas sensing applications, we are specifically interested in radiation within the absorption spectrum of the chemical species under study. For  $\text{CO}_2$ , we target the  $[4.16 - 4.36]\mu\text{m}$  spectral window. We consider that electro-thermal Joule ohmic conversion is total, and focus on the thermo-optical one. In our system, heat can be dissipated in two ways: by conduction to the substrate through the arms (equation (8)), or by radiation (equation (9)). Equation (9) is equivalent to Eq.(4) integrated over the surface in the case where  $\varepsilon$  is independent of the wavelength.

$$\varphi_{\text{cond}}(t) = \frac{(T(R, t) - T_{\text{sub}})}{Z_a} N_a w_a e \quad (8)$$

$$\varphi_{\text{rad}}(t) = 2\pi\sigma\varepsilon \int_0^R (T(r, t)^4 - T_{\text{sub}}^4) r dr \quad (9)$$

From these two formulas, one can observe that conduction scales linearly with temperature, whereas radiation scales with its fourth power. As a consequence, temperature is the most important parameter controlling the ratio between conduction and radiation. However, in standard free-standing membranes, temperature is often limited, to avoid material premature degradation<sup>7</sup>. The second most important parameter of the structure is the radius of the central disk, as radiation is proportional to the area of the source ( $\propto R^2$ ), while conduction is proportional to its perimeter ( $\propto R$ ). Accordingly, larger membranes are more efficient than smaller ones. With that scaling in mind, very large membrane have been proposed and studied<sup>8</sup>. Not to mention that mechanical resistance would be critical, this kind of device needs a lot of power to get to, and be maintained at its working temperature. In low power applications, energy per measurement and maximum power are fundamental constraints, and tend to prohibit the use of energy intensive solutions. Generally speaking, increasing the size of the membrane is achieved at the price of an increased electrical peak power, thus reducing the time it is on. A compromise has to be found in order to optimally use available energy and reach the best efficiency in the desired spectral window.

### 3.2 Case study

In this part, we consider specifically the membrane developed by Barritault *et al*<sup>9</sup>. It consists of two 100nm thick  $\text{Si}_3\text{N}_4$  layers embedding a TiN(10nm)/Pt(30nm)/TiN(10nm) sandwich serving as metallic tracks (Fig. 2a,b). The TiN layers act as diffusion barriers for Pt. A 100nm  $\text{SiO}_2$  layer is also located in the stack to mitigate the mechanical constraints between the different layers. The total thickness of the structure is  $e = 350\text{nm}$ . Default radius is  $75\mu\text{m}$ , and the structure is suspended by two arms of width  $w_a = 30\mu\text{m}$  and length  $L_a = 150\mu\text{m}$ . The thermal resistivity of the arms is  $Z_a = 1.49 \cdot 10^{-4} \text{K} \cdot \text{W}^{-1} \cdot \text{m}^2$ . Figure 2 presents a Scanning Electron Microscope (SEM) image of the membrane. The thermal properties of the materials are detailed in Table 1. The structure is supposed to behave like a blackbody, thus radiating with a unit emissivity in the whole spectrum, which is an acceptable assumption for this stack around 3-10  $\mu\text{m}$ .

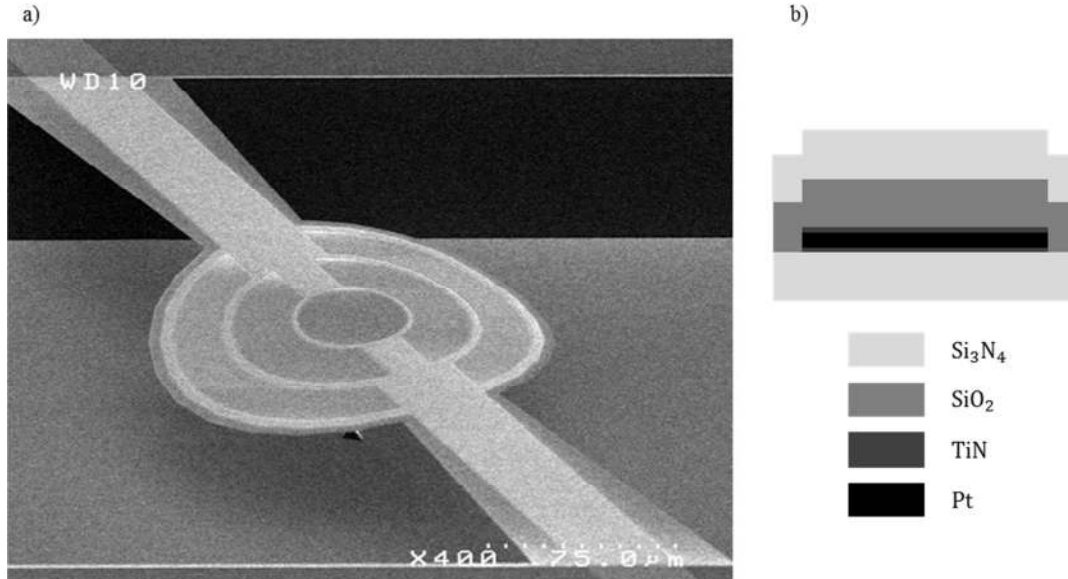


Figure 2: a) SEM image of the suspended membrane<sup>9</sup>. Although not visible on this picture, the microhotplate comprises temperature homogenisers between the electric tracks. b) Scheme of the stack

Table 1: Material and membrane physical properties at room temperature (300K). Temperature dependence is neglected.

	Thickness (nm)	Density (kg.m <sup>-3</sup> )	Specific heat capacity (J.kg <sup>-1</sup> .K <sup>-1</sup> )	Thermal conductivity (W.m <sup>-1</sup> .K <sup>-1</sup> )
Si <sub>3</sub> N <sub>4</sub>	200	3100 <sup>10</sup>	700 <sup>10</sup>	2.6 <sup>11</sup>
SiO <sub>2</sub>	100	2200 <sup>10</sup>	1000 <sup>10</sup>	1.2 <sup>11</sup>
TiN	20	5400 <sup>12</sup>	545 <sup>12</sup>	19.2 <sup>12</sup>
Pt	30	21450 <sup>13</sup>	131 <sup>13</sup>	58 <sup>11</sup>
Total/Weighted mean	350	4547	728	7.9

This micromembrane is typically operated at  $T_f = 650^\circ\text{C}$ , as higher temperatures can strongly reduce its lifetime. The available energy per measurement is a first specification constraint. It can be obtained from the total energy capacity of the operating battery divided by the number of measurements in the desired lifetime. Using a standard 1.5V AA battery (2.6Wh, or 9360J), a 10 years expected lifetime and 3mn repetition rate, we get  $E = 5\text{mJ}$  per measurement. This calculation does not take into account self-discharge, which should be accounted for in a rigorous analysis. Moreover, due to the internal resistance of the battery  $R_{\text{int}}$  (typically a fraction of an ohm) the maximum power that can be delivered is limited, calling for a second specification constraint. The load has to be kept at least ten times larger than this internal resistance to work properly along the battery lifetime (energy should be dissipated in the system rather than in the battery itself). In this case, this maximum power is approximately 1W, which means that the membrane cannot be heated faster than  $t = 5\text{ms}$ .

### 3.3 Calculations

The thermal simulations are undertaken via a Matlab routine implementing differential equations (3)-(7). For a given membrane radius, the power source  $P$  is adjusted to reach the maximum temperature without exceeding it. Formally, this is just an extra boundary condition for the set of equations. Given the energetic constraint, the source produces an increasing amount of radiation as time goes, until exhaustion of the energy “quantum”, being thus turned on during a time  $t = E/P$  until switch-off. This time  $t$  depends on the radius  $R$ , thus the above conditions implicitly define a  $t(R)$  or  $R(t)$  law. From the spatio-temporal distribution of temperature till cool down, time-integrated energy losses are computed (conduction, total radiation and radiation in the spectral window of interest). Those quantities eventually help us calculating the spectral efficiency  $\eta_\lambda$  according to:

$$\eta_\lambda = \frac{E_{\text{rad}\lambda}}{E} = \frac{E_{\text{rad}\lambda}}{E_{\text{rad}} + E_{\text{cond}}} \quad (10)$$

where  $E_{\text{rad}\lambda}$  is the energy radiated in the  $[4.16 - 4.36]\mu\text{m}$  window. Figure 3c shows this efficiency calculated along the  $R(t)$  line verifying both temperature and energy conditions.

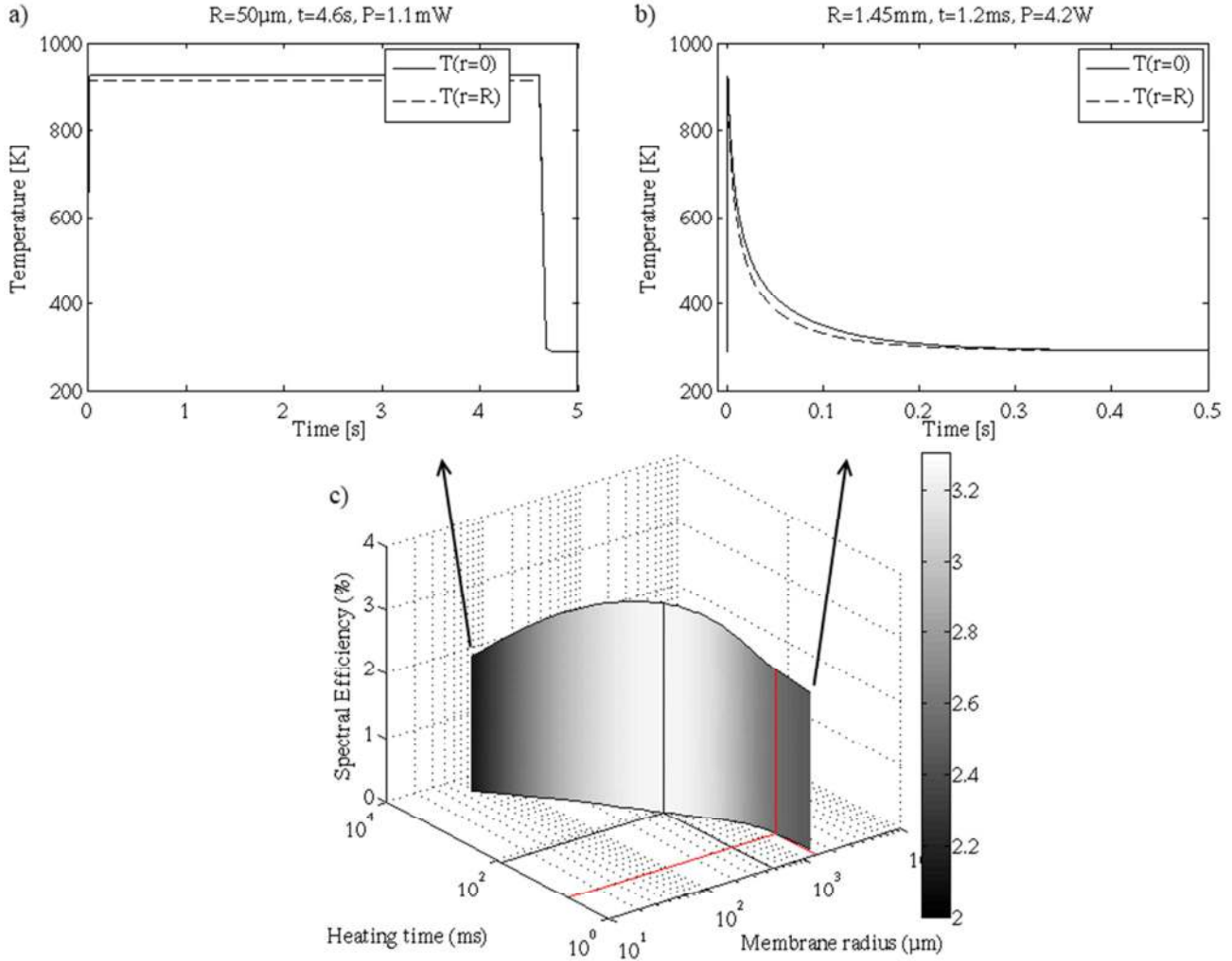


Figure 3 : a) Temporal temperature profile for a small (50µm) membrane heated during a long time (4.6s) with small power (1.1mW) b) Temporal temperature profile for a large (1.45mm) membrane heated during a short time (1.2ms) with large power (4.2W) c)  $R(t)$  solutions of the constrained thermal equations with  $E = 5\text{mJ}$  and  $T_f = 923\text{K}$  and corresponding spectral efficiency (height/color of curtain). The black lines indicate the optimum and the red ones outline the power limitations ( $t = 5\text{ms} \equiv P = 1\text{W}$ ).

Two extreme regimes are observed:

- When considering a small radius (Figure 3a), steady state is rapidly achieved, meaning the supply power must equal the cw losses:  $P = P_{\text{losses}} = P_{\text{cond}} + P_{\text{rad}} \approx N_a w_a e^{\frac{(T_f - T_{\text{sub}})}{Z_a}} + \pi R^2 \sigma \varepsilon (T_f^4 - T_{\text{sub}}^4)$  if the membrane is isothermal. This power being relatively small, the source can be operated during a long time. The efficiency decreases when the radius decreases, in agreement with considerations presented in 3.1.
- Inversely, a large membrane (Figure 3b) consumes almost all of its energy to get to the right temperature before any sizable loss intervenes (even radiative), and is fully operated in transient state, mostly when cooling:  $E = \pi R^2 e \rho C_p (T_f - T_{\text{sub}})$ . This simple behavior sets an upper limit  $R_{\text{max}}$  on the radius of the membrane, from compliance with temperature and energy constraints. Moreover, heating has to be quicker when the radius increases in order to limit the losses. Maximum power delivered by the battery thus becomes an issue. In this case, the membrane is not kept at the higher temperature for a long time, and a significant lowering of the efficiency is observed.

Between these two regimes, there is a compromise yielding the best efficiency. In this case, it corresponds to a membrane with radius  $R = 475\mu\text{m}$  heated by  $P = 58\text{mW}$  during  $t = 86\text{ms}$ . The spectral efficiency reaches 3.3%, to be compared with the 2.4% of the initial  $75\mu\text{m}$  radius membrane. Better efficiency can hardly be achieved, given that for this optimal situation more than 90% of the total supplied power is already radiated by the membrane. The maximum value of efficiency is given by the proportion of the blackbody radiance located in the spectral window of interest ( $[4.16 - 4.36]\mu\text{m}$ ) which is approximately 3.5% for a temperature of 923K. The easiest way to achieve higher efficiencies is then to tailor the emissivity of the structure, so as to level up this 3.5%.

### 3.4 Influence of emissivity tailoring

As seen in the previous section, the radiative efficiency for micro-hotplates is relatively small, on the order of a few percent. One interesting lead is to tailor the membrane emissivity, to favor the radiation in the spectral window of interest. Different approaches have already been studied, a lot of them based on plasmonic resonators. Metal Insulator Metal (MIM) structures have proven to provide a wide-angle, narrow band emission<sup>14-18</sup>. Other possibilities based on photonic crystals<sup>19</sup> or more exotic structures<sup>20</sup> have also been proposed. However, plasmonic structures have the advantage of being composed of very thin layers, which is important in terms of thermal load if they have to be deposited on top of the membrane. Here, we consider an optimal “top-hat” spectral emissivity, that is:

$$\begin{aligned} \varepsilon(\lambda) &= 1 \quad \forall \lambda \in [4.16 \text{ } 4.36]\mu\text{m} \\ \varepsilon(\lambda) &= 0 \quad \text{elsewhere} \end{aligned} \tag{11}$$

Although not truly achievable, this extreme case provides a good understanding of mechanisms occurring in non-blackbody materials. Actual tailored emissivity will have efficiencies between the blackbody one and the optimal one. The corresponding  $R(t)$  solution and its efficiency trend are given in Figure 4 and compared with that obtained in Figure 3c with unitary emissivity. A strong improvement is observed.

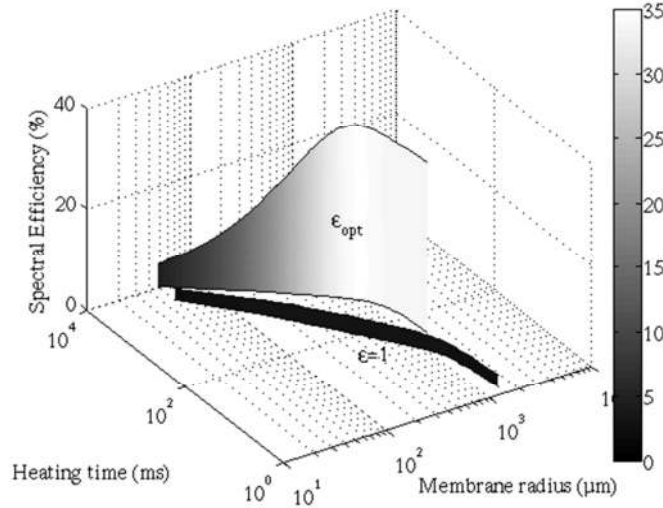


Figure 4:  $R(t)$  solution and corresponding spectral efficiency of the constrained thermal equations with  $E = 5\text{mJ}$  and  $T_f = 923\text{K}$  for the optimal emissivity defined in equation (12) and the unitary emissivity also plotted in Figure 3c.

A much higher efficiency up to 35% is achieved in this case, the limiting factor being the power lost through conduction. This limit depends directly on the radius of the source, itself being a function of the available energy per measurement. At a given radius, the membrane with tailored emissivity can be heated much longer than the basic one, due to the global reduction of radiative power loss. The power needed to keep the micromembrane at  $T_f$  is thus significantly reduced. The main drawback is the increase of the rise time  $t_r$  of the source. If losses can be neglected during rise time, the latter can be computed as the ratio between the energy stored in the device and the supply power:  $t_r = E/P = \pi R^2 \rho C_p (T_f - T_{\text{sub}})/P$ . As it scales with  $P^{-1}$ , the decrease in power leads to a reduction of the source bandwidth. Moreover, the emissivity enhancement is most likely to be achieved by adding a layer on top of the membrane. In this case, the thickness  $e$  of the membrane will increase, emphasizing this reduction of bandwidth.

## 4. CONCLUSION

In this paper, we presented a simple 1D-model for the thermo-optical modeling of suspended micro-membranes, for e.g. thermal infrared sources in gas sensor applications. Starting from down-to-earth constraints such as available energy per measurement and maximum supply power, we demonstrated that there is a compromise between the size of the membrane and the time it has to be heated, which yields the best efficiency. The limit imposed by the broad blackbody radiation spectrum can be overcome by using tailored emissivity, adding for example a thin active layer on top of the membrane. In this case, much higher efficiencies are expected, albeit at the price of a reduced bandwidth. Coupled thermal conductive and radiative phenomena have been described and clarified, and should provide a helpful tool for the design of such kind of radiative sources.

## REFERENCES

- [1] Demarne, V., and Grisel, A., “An integrated low-power thin-film CO gas sensor on silicon,” *Sensors and Actuators* 13(4), 301–313 (1988).
- [2] Bauer, D., Heeger, M., Gebhard, M., and Benecke, W., “Design and fabrication of a thermal infrared emitter,” *Sensors and Actuators A: Physical* 55(1), 57–63 (1996).
- [3] Ali, S.Z., Udrea, F., Milne, W.I., and Gardner, J.W., “Tungsten-Based SOI Microhotplates for Smart Gas Sensors,” *Journal of Microelectromechanical Systems* 17(6), 1408–1417 (2008).
- [4] Khan, U., and Falconi, C., “Temperature distribution in membrane-type micro-hot-plates with circular geometry,” *Sensors and Actuators B: Chemical* 177, 535–542 (2013).
- [5] Khan, U., and Falconi, C., “Micro-hot-plates without simply connected hot-spots and with almost-circular temperature distribution,” *Sensors and Actuators B: Chemical* 185, 274–281 (2013).
- [6] Saxena, G., and Paily, R., “Analytical Modeling of Square Microhotplate for Gas Sensing Application,” *IEEE Sensors Journal* 13(12), 4851–4859 (2013).
- [7] Mele, L., Santagata, F., Iervolino, E., Mihailovic, M., Rossi, T., Tran, A.T., Schellevis, H., Creemer, J.F., and Sarro, P.M., “A molybdenum MEMS microhotplate for high-temperature operation,” *Sensors and Actuators A: Physical* 188, 173–180 (2012).
- [8] Brucoli, G., Bouchon, P., Haïdar, R., Besbes, M., Benisty, H., and Greffet, J.-J., “High efficiency quasi-monochromatic infrared emitter,” *Applied Physics Letters* 104(8), 081101 (2014).
- [9] Barritault, P., Brun, M., Gidon, S., and Nicoletti, S., “Mid-IR source based on a free-standing microhotplate for autonomous CO<sub>2</sub> sensing in indoor applications,” *Sensors and Actuators A: Physical* 172(2), 379–385 (2011).
- [10] Soboyejo, W.O., and Srivatsan, T.S., [Advanced Structural Materials: Properties, Design Optimization, and Applications], CRC Press (2006).
- [11] Cozzani, E., Roncaglia, A., Zampolli, S., Elmi, I., Mancarella, F., TAMARRI, F., and Cardinali, G.C., “Material Properties Measurement and Numerical Simulation for Characterization of Ultra-Low-Power Consumption Hotplates,” in *Solid-State Sens. Actuators Microsyst. Conf. 2007 TRANSDUCERS 2007 Int.*, 1661–1664 (2007).
- [12] Pierson, H.O., [Handbook of Refractory Carbides & Nitrides: Properties, Characteristics, Processing and Apps.], William Andrew (1996).
- [13] Cardarelli, F., [Materials Handbook: A Concise Desktop Reference], Springer (2008).
- [14] Diem, M., Koschny, T., and Soukoulis, C.M., “Wide-angle perfect absorber/thermal emitter in the terahertz regime,” *Physical Review B* 79(3), 033101 (2009).
- [15] Liu, N., Mesch, M., Weiss, T., Hentschel, M., and Giessen, H., “Infrared Perfect Absorber and Its Application As Plasmonic Sensor,” *Nano Letters* 10(7), 2342–2348 (2010).
- [16] Liu, X., Tyler, T., Starr, T., Starr, A.F., Jokerst, N.M., and Padilla, W.J., “Taming the blackbody with infrared metamaterials as selective thermal emitters,” *Physical review letters* 107(4), 45901 (2011).
- [17] Mason, J.A., Smith, S., and Wasserman, D., “Strong absorption and selective thermal emission from a midinfrared metamaterial,” *Applied Physics Letters* 98(24), 241105 (2011).
- [18] Puscasu, I., and Schaich, W.L., “Narrow-band, tunable infrared emission from arrays of microstrip patches,” *Applied Physics Letters* 92(23), 233102–233102–3 (2008).
- [19] Celanovic, I., Perreault, D., and Kassakian, J., “Resonant-cavity enhanced thermal emission,” *Physical Review B* 72(7), 075127 (2005).
- [20] Drevillon, J., Joulain, K., Ben-Abdallah, P., and Nefzaoui, E., “Far field coherent thermal emission from a bilayer structure,” *Journal of Applied Physics* 109(3), 034315–034315 (2011).